Continuum Mech. Thermodyn. (2024) 36:289–297
https://doi.org/10.1007/s00161-022-01093-9

ORIGINAL ARTICLE

M. Zaghdoudi · A. Kömmling · M. Jaunich · D. Wolff

Oxidative ageing of elastomers: experiment and modelling

Received: 23 September 2021 / Accepted: 5 March 2022 / Published online: 2 April 2022

Abstract During an extensive test programme at the Bundesanstalt für Materialforschung und prüfung, material property changes of EPDM O-rings were investigated at different ageing times and two ageing temperatures of 125 ° C and 150 ° C. To exclude possible diffusion-limited oxidation (DLO) effects that can distort the data, IRHD microhardness measurements were taken over the cross section of compressed O-rings. Continuous stress relaxation measurements were taken on samples free of DLO effects. The additional effect of physical processes to irreversible chemical ones during a long-term thermal exposure is quantified by the analysis of compression set measurements under various test conditions. By combining the different experimental methods, characteristic times relative to the degradation processes were determined. On the basis of experimental data, a microphysically motivated model that takes into account reversible and irreversible processes was developed. The parameter identification strategy of the material model is based on our experimental investigations on homogeneously aged elastomer O-rings. The simulated results are in good agreement with the experiments.

Keywords Compression stress relaxation · Compression set · IRHD microhardness · Modelling

1 Introduction

Faced with increasing market competitiveness as well as consumption, manufacturers must guarantee a long service life of their components. Elastomers are among these components. They are used in various fields and different industrial applications [1]. In high safety demanding applications (e.g. hydrogen infrastructure [2] or containers for radioactive materials [3]) in addition to long-term effects, the safety assessment also raises the question of lifetime predictions and failure behaviour under extreme conditions. Probably the most encountered conditions to which the elastomer seal is exposed to are mechanical loading, temperature, and oxygen [4]. The combination of elevated temperature and oxygen leads to thermo-oxidative ageing which degrades the material properties over exposure time. The degradation is irreversible and microstructural changes (chain scission and crosslinking) occur during thermo-oxidative ageing [5–7]. Since accelerated ageing experiments are sometimes very long and therefore costly, numerical simulations have gained further importance. According to the two-network theory, continuous stress relaxation is a measure of chain scission, while continuous stress relaxation subtracted from intermittent stress relaxation at each ageing time is a measure of crosslinking [8,9]. Inspired by the two-network theory very interesting modelling approaches were developed [10–13].

On the other hand, experimental compression stress relaxation (SR) and compression set (CS) present key indicators of elastomer seal's long-term performance and are often used for lifetime predictions. However,

Communicated by Andreas Öchsner.

M. Zaghdoudi (✉) · A. Kömmling · M. Jaunich · D. Wolff
Bundesanstalt für Materialforschung und -prüfung, 12200 Berlin, Germany
E-mail: Maha.zaghdoudi@bam.de

care must be taken when analyzing the data as diffusion-limited oxidation effects (DLO) may appear [14]. DLO effects occur when the oxygen in the interior of the sample is consumed faster than it can diffuse in from the surrounding air. This can lead to oxygen shortage in the core of the sample and thus to less ageing in the core region. This heterogeneous ageing may distort the ageing data and can result in misleading lifetime predictions.

Moreover, during SR physical (reversible) and chemical (irreversible microstructural changes) processes take place [4]. To separate physical and chemical processes during SR, most experiments were performed either in inert atmosphere or first at low temperature or short time and then the resulting relaxation is subtracted at high temperature or longer time by using the time-temperature superposition technique [15–17]. In this paper, a new approach to separate physical and chemical processes that occur during stress relaxation is proposed through the analysis of compression set measurements under various test conditions. Characteristic times with regard to the degradation processes are then determined by examining CS measurements and compression SR measurements. These times are then used in the identification of material parameters in the simulation section based on the model of Shaw et al. [13] that was motivated by the two-network theory of Tobolsky [8,9].

2 Experimental

2.1 Material

Commercial ethylene-propylene-diene rubber (EPDM) O-rings with a cord diameter of 10 mm and an inner diameter of 190 mm were used. The peroxide cured EPDM is based on a polymer containing 48 wt% ethylene, 4.1 wt% ethylidene norbornene (ENB) and was compounded with 90 phr of carbon black filler, and no plasticizer.

2.2 IRHD

IRHD measurements were taken on O-ring cross sections as shown in Fig. 1 across the sample profile using a linear table according to DIN ISO 48-2:2021-02 with the method M. As the O-rings cross sections are thick (10 mm), ageing can be influenced by diffusion-limited oxidation (DLO) effects. Slices of O-rings with a thickness of 3–4 mm were cut from O-rings that had been aged at 125 ° C and 150 ° C compressed by 25%, respectively. The measuring points on the cross section are illustrated in Fig. 1. Only x direction will be considered as the outsides on the left- and the right-hand side were in direct contact with oxygen during ageing in the compressed state.

2.3 Compression set

CS was measured at room temperature on EPDM O-ring segments aged compressed by 25% at 125 ° C and 150 °C for different ageing times ranging from 1 to 185 d as shown in Fig. 2. The measurements were taken 30 min after disassembly according to standards ASTM D395-18 and DIN ISO 815-1:2016-09 and for different times after disassembly for up to 1 year. This showed that the recovery proceeds even after several days. Therefore to accelerate the recovery towards equilibrium [18], the O-ring segments were placed in an oven for 1 day at 100 ° C and the recovered height after thermal conditioning was measured. For each type of

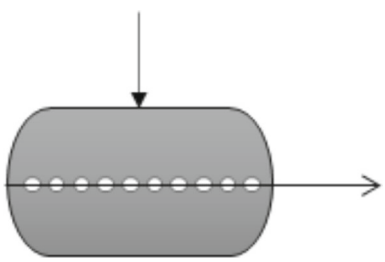

Fig. 1 IRHD microhardness measuring positions across O-ring cross section

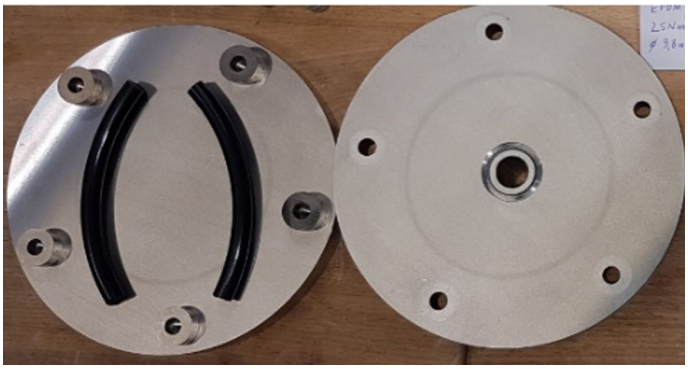

Fig. 2 O-ring segments between flanges for CS measurements

CS measurement, the recovered height of O-ring segments was measured at 7–10 positions using a calliper and CS was calculated from the average values.

2.4 Continuous stress relaxation

Continuous SR measurements were taken at 125 ° C and 150 ° C on O-ring segments with a length of approximatively 40 mm. The O-ring segments were thermally and mechanically conditioned according to the standard DIN ISO 3384:2008. Three O-ring segments were tested using the SR rigs EB 02 in a cell oven EB 22 from Elastocon. The median curve of three measurements will be presented and is expressed as the ratio R_c of the continuously measured force F_c to the initial force F_0. F_0 is the measured force 30 min after the full compression by 25% was achieved according to the DIN ISO 3384:2008.

3 Modelling

Within the framework of large deformation of hyper-elastic quasi-incompressible materials, the strain energy function is split into a deviatoric and volumetric part as expressed in Eq. (1).

$$\Psi\left(\boldsymbol{B}\right) = \overline{\Psi}\left(\boldsymbol{B}\right) + \Psi^{\mathrm{vol}}\left(J\right) \tag{1}$$

$\boldsymbol{B}$ is the left Cauchy green tensor and J is the transformation Jacobian. $\boldsymbol{B}$ is expressed in terms of the multiplicative decomposition as:

$$\boldsymbol{B} = \bar{\boldsymbol{B}}.\boldsymbol{B}^{\mathrm{vol}} \tag{2}$$

Since the applied strains are not large (25%), the simplified Neo–Hook potential is adopted. On the one hand, the model has a physical meaning as it is based on the statistical thermodynamics of crosslinked polymer chains. On the other hand, the Neo-Hook potential has already proven its accuracy to model the material behaviour during thermo-oxidative ageing [19].

$$\Psi\left(\boldsymbol{B}\right) = C.\left(\mathrm{tr}\left(\bar{\boldsymbol{B}}\right) - 3\right) + \frac{1}{D}\left(J-1\right)^2 \tag{3}$$

where $C = \frac{1}{2} n\left(t\right) \cdot k \cdot T$.

$n\left(t\right)$ is the effective number of crosslinks as a function of exposure time t, k is Boltzmann's constant, T is the absolute temperature and $D = 2/K_0$ where K_0 is the initial bulk modulus.

Physical relaxation is a reversible process and is due to chain rearrangement under compression load. In a real system, chemical degradation and physical relaxation occur simultaneously during ageing, but physical relaxation is dominant at lower ageing times and chemical relaxation on the other hand is preponderant at longer ageing times [20]. In modelling, it is possible either to separate the variables (physical and chemical) [13] or to couple them. The coupling can be used when the experimental basis required to identify the coupling parameters is available (e.g. intermittent ageing in oxygen and inert atmosphere). In this paper, the stress relaxation is presented as an additive contribution of the physical and chemical relaxation.

The short-term physical relaxation in a standard static analysis and, under isothermal conditions, corresponds to an elastic solution based on instantaneous elastic moduli (Eq. 4). Here the relaxation coefficients are applied to the constant C that define the energy function in Eq. (3).

$$C^R(t) = C^0 \cdot \left(1 - \sum_{k=1}^{n} \bar{g}_k^p \cdot \left(1 - \exp\left(-t/\tau_k\right)\right)\right) \tag{4}$$

where $C^0 = \frac{1}{2} n(0) \cdot k \cdot T$ and $\bar{g}_k^p$ and τ_k are the Prony parameters.

To take into account chemical ageing, the effective number of crosslinks n is chosen as a decreasing function of t according to the proposed function of Shaw et al. [13] so that the Cauchy stress is given in Eq. (5). Here, a number of first-order chemical relaxation processes take place simultaneously, each one of which is Maxwellian. Each process (i) has a characteristic time τ_i which is evolved with a portion of the network interpreted as a phase fraction A_i.

$$\sigma^c(t) = \frac{n_0 . \sum_{i=1}^{n} A_i \exp(-t/\tau_i) k.T}{J} \left(\bar{\boldsymbol{B}} - \frac{1}{3} tr\left(\bar{\boldsymbol{B}}\right).\mathbf{1}\right) + \frac{2}{D}(J-1).\mathbf{1} \tag{5}$$

where $A_i \geq 0$ and $\sum_{i=1}^{n} A_i = 1$.

From Eqs. (4) and (5), the total Cauchy stress $\sigma(t)$ is expressed as:

$$\sigma(t) = \frac{n_0 . k . T . (1 - \sum_{k=1}^{n} \bar{g}_k^p \cdot (1 - \exp(-t/\tau_k)) + \sum_{i=1}^{n} A_i \exp(-t/\tau_i))}{J} \left(\bar{\boldsymbol{B}} - \frac{1}{3} tr\left(\bar{\boldsymbol{B}}\right).\mathbf{1}\right) + \frac{2}{D}(J-1).\mathbf{1} \tag{6}$$

4 Results

IRHD microhardness measurements were taken over the cross section of compressed O-rings aged at 125 °C and 150 °C according to DIN ISO 48-2:2021-02 with the method M. The development over time is shown in Fig. 3. The microhardness profiles show no changes for samples aged up to 909 d at 125 °C and 75 d at 150 °C. For samples aged at 125° C for 1093 d and those aged at 150 °C for 101 d, slight DLO effects are detected. This is clearly emphasized in Fig. 3 as the measured values of microhardness near the surface are higher than those measured in the interior of the O-ring cross section. The microhardness profiles of EPDM aged at 125 °C present slight decrease of maximum 2 Shore D Hardness in the core region between 909 and 1093 d which might be due to anaerobic chain scission reactions.

CS was measured 30 min after disassembly according to ASTM D395-18 and DIN ISO 815-1:2010 and after 0.5 d, 1 d, 5 d, 10 d, 18 d, 50 d and 365 d. An exemplary result of the CS measurement of EPDM aged at

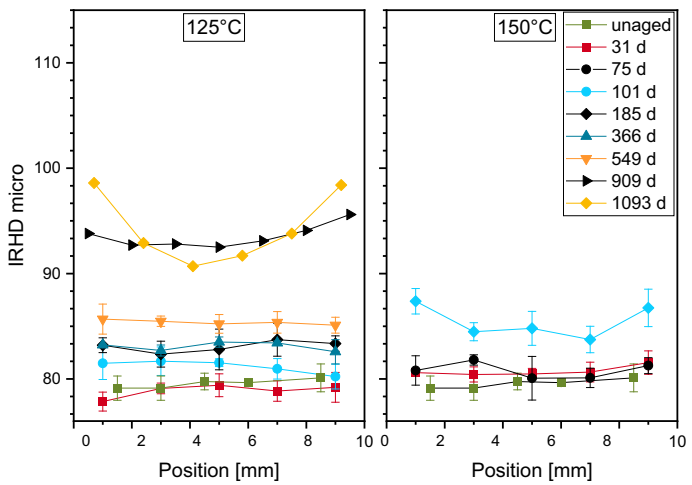

Fig. 3 IRHD microhardness measurements at 125 °C and 150 °C at different ageing times

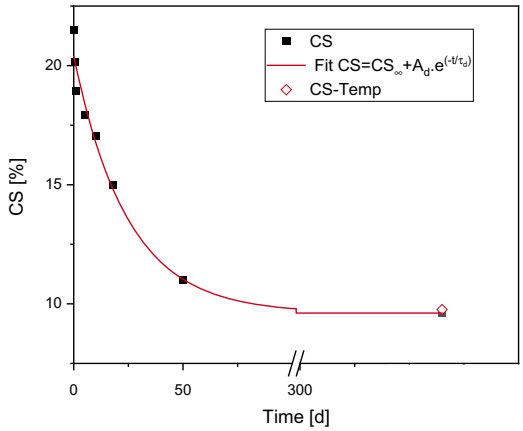

Fig. 4 Evolution of the recovery of EPDM aged at 125 ° C for 10 d over time and its corresponding fit

125 ° C for 10 d is presented in Fig. 4. It shows the evolution of the recovery over time and its corresponding fit ($CS = CS_\infty + A_d \cdot e^{-t/\tau d}$). The calculated errors of measurements are within the size of the used symbols. The measured CS after thermal conditioning reflects only the irreversible chemical reactions (chain scission and crosslinking), and its value is set as CS_∞. According to our investigation, it corresponds to about 1-year recovery time as the difference between the measured CS after 1 year and the measurement after tempering is 0.1%. The term $A_d \cdot e^{-t/\tau d}$ accounts for reversible physical processes. A_d and τ_d are the retardation strength and the characteristic time at a given ageing time, respectively. For 10 d ageing at 125 ° C, $A_d = 10.8$ and $\tau_d = 24.7$ d with a good correlation fit ($R^2 = 0.98$). It is to mention that two representative samples were previously tempered again [21] in order to confirm that the CS after the first tempering corresponds to the equilibrium value CS_∞ and the results after first and second tempering were almost the same. The results of CS at different times after disassembly that are presented in Fig. 4 call into question the test method according to the standard (ASTM D395-18 - DIN ISO 815-1:2010) as the recovery proceeds further after 30 min after disassembly. A common error of the measurements is about ± 3% [22]. From the results of Fig. 4, the difference in percent between a measurement after 30 min and CS_∞ is about 59%. These differences should be considered when comparing tempered CS results to those measured with the standard procedure.

Figure 5a, b shows the evolution of CS measurements at 125 ° C and 150 ° C after 30 min and after thermal conditioning over ageing time, respectively, which illustrates again their different values. In Fig. 5b, the values of CS after ageing at 101 d which are marked with a blue frame will not be taken into account for further analysis as these samples exhibited slight DLO effects according to the IRHD microhardness profiles shown in Fig 3. In Fig. 5a, b, the normalised relaxation R_c over ageing time is also presented at 125 ° C and 150 ° C. R_c exhibits two regions that could be approached asymptotically [23]. For the first region, the line was obtained by fitting a tangent to the linear region starting from the first recorded value of R_c. The second line was obtained by fitting a tangent to the half-time relaxation at 50% force loss $t_{50\%}$ ((*) in Fig. 5a, b). The first region correlates with physical relaxation [23]. Its duration t_{physical} ((+) in Fig. 5a, b) is defined as the time at which the measurement data deviate by 1% from the straight line. The second phase is associated with chain scission reactions [23]. The induction time $t_{\text{induction}}$ which represents the onset of the dominant chemical reactions can be estimated from the intersection of the two linear regions [22]. It is noteworthy to clarify that the induction time ($t_{\text{induction}}$) should not be confused either with the induction period in chemistry which is an initial slow stage of chemical reaction or the oxidative induction time (OIT) which is determined by means of Fourier transform infrared spectroscopy (FTIR), chemiluminescence (CL) or differential scanning calorimetry (DSC). The latter is described in ASTM D3895-07. The induction time here represents the threshold from which chain scission during the continuous SR test is noticeable. The threshold was previously confirmed for EPDM aged at 125 ° C by comparing the continuous and intermittent SR measurements [22] that represent the evolution of chain scission and crosslinking according to the two-network theory of Tobolsky [8,9]. It has been shown for EPDM that the influence of chain scission reactions competes with that of crosslinking at longer ageing times. Moreover, chain scission and crosslinking were occurring with approximately equal impact until 10 d for EPDM aged at 125 ° C [22], which is the determined threshold in Fig. 5a. At a macromolecular scale, the induction time represents the time at which the concentration of the oxidative products is sufficiently high to accelerate the decomposition. In fact, during thermo-oxidative ageing, macromolecules are mostly cleaved

Table 1 Set of parameters used in the simulation

Physical relaxation parameters			Chemical relaxation parameters			
	$\bar{g}_k^p$	$\tau_k(\mathrm{d}^{-1})$	A_1	A_2	τ_1 (d^{-1})	$\tau_2(\mathrm{d}^{-1})$
Temperature						
125 ° C	0.0043	0.003	0.12	0.85	3.8	205
	0.03	0.3				
150 ° C	0.0043	0.003	0.11	0.87	0.64	26
	0.03	0.3				

by the β-scission process to fragments with ketone and vinyl end-groups. In the early reaction stages, these oxidation products are only formed to a certain extent. However, at a certain ageing time (induction time) when the concentration of these products is increased enough, their more energy-efficient bimolecular decomposition begins [24].

To compare CS and R_c, a correction factor is used [25] since CS measurements were taken at room temperature (RT = 23 ° C), but R_c measurements at 125 ° C and 150 ° C. A linear expansion coefficient of 2.10^{-4}/K was previously determined by the Dynamic Mechanic Thermal Analysis (DMTA) between room temperature and the test temperature [22]. For a temperature difference of 102 ° C and 127°C which are the differences between the ageing temperature and the RT, the correction factors are 0.944 and 0.99, respectively. By using the correction approach, the R_c at 125 ° C and 150 ° C can be compared to the corrected equilibrium compression set and the corrected CS after 30 min at each ageing time. Figure 5c, d illustrates the evolution of R_c versus the corrected CS after 30 min and CS after tempering for EPDM O-rings aged at 125 ° C and 150 ° C, respectively. The data represented in a blue frame in Fig. 5d will not be analysed due to DLO effects as stated before. The evolution (Fig. 5c, d) is linear, and the contribution of physical and chemical processes is determined through the analysis of the corrected CS after tempering. The intercept of the linear fit of R_c versus CS after tempering with R_c ((X) in Fig. 5c, d) corresponds to the shift factor to which the R_c curve should be moved if only irreversible chemical relaxation is to be considered. This intercept represents the value at which irreversible chemical degradation begins. The difference between the shifted curve and the real one ($\sim$ 10% for the ageing temperature of 125 ° C) accounts for the physical processes that occur during ageing. The ageing time corresponding to R_c intercept represents the initiation time $t_{\mathrm{initiation}}$ of the chemical degradation and is determined from Fig. 5a, b. Again, the induction period ($t_{\mathrm{induction}}$) is very long and lasts 10 d and 2 d for EPDM aged at 125° C and 150° C, respectively. On the other hand, the initiation time starts earlier. The determined characteristic times ($t_{\mathrm{physical}} = 0.06$ d, $t_{\mathrm{initiation}} = 1$ d, $t_{\mathrm{induction}} = 10$ d and $t_{50\%} = 69$ d) are intrinsic only for the investigated rubbers (geometry and compounds) at the ageing temperature of 125 ° C. For 150° C the characteristic times are $t_{\mathrm{physical}} = 0.05$ d, $t_{\mathrm{initiation}} = 0.13$ d, $t_{\mathrm{induction}} = 2$ d and $t_{50\%} = 25$ d.

Since the determined $t_{\mathrm{initiation}}$ is representative for the initiation time of the chemical degradation, the experimental results of SR shown in Fig. 5a, b until 1 d and 0.13 d relative to the ageing temperatures of 125 ° C and 150 ° C are introduced in the ABAQUS® simulation software in order to determine the parameters of physical relaxation. An internal calibration tool identifies the Prony parameters according to Eq. (4) until the given initiation time.

For chemical stress relaxation, two first-order Maxwellian chemical relaxation processes are applied in Eq. (5). The material parameters used in the simulation of physical and chemical relaxation are summarised in Table 1. The physical relaxation parameters ($\bar{g}_k^p$ and τ_k) for samples aged at 125 ° C and 150 ° C are the same even when the initiation of the chemical degradation happens at different times ($t_{\mathrm{initiation}} = 1$ d for 125 ° C and $t_{\mathrm{initiation}} = 0.13$ d for 150° C). On the other hand, the chemical relaxation times τ_1 and τ_2 (that represent early and later degradation, respectively) differ due to the different reaction rates at 125 ° C and 150 ° C. The shift factor between 125 ° C and 150 ° C is 5.9 for τ_1 and 7.9 for τ_2. Moreover, when we examine the SR experimental results shown in Fig. 5a, b, the 150 ° C curve can be shifted to the 125 ° C curve until superposition with a shift factor of 6.9 (considering the whole relaxation process). This represents the macroscopic average of the superposition factors of low and high chemical relaxation times. The simulation results of the normalised continuous stress relaxation of EPDM aged at 125 ° C and 150 ° C with physical relaxation and chemical ageing are shown in Fig. 6 and exhibit very good agreement with the experimental data.

The experimental SR results were performed at 125 ° C and 150 ° C until a degradation stage of $R_c = 0.47$ (ageing time = 173 d) and $R_c = 0.04$ (ageing time = 120 d), respectively. At this degradation stage no DLO effects were detected for samples aged at 125 ° C as shown in Fig. 3. Since the proposed model and its

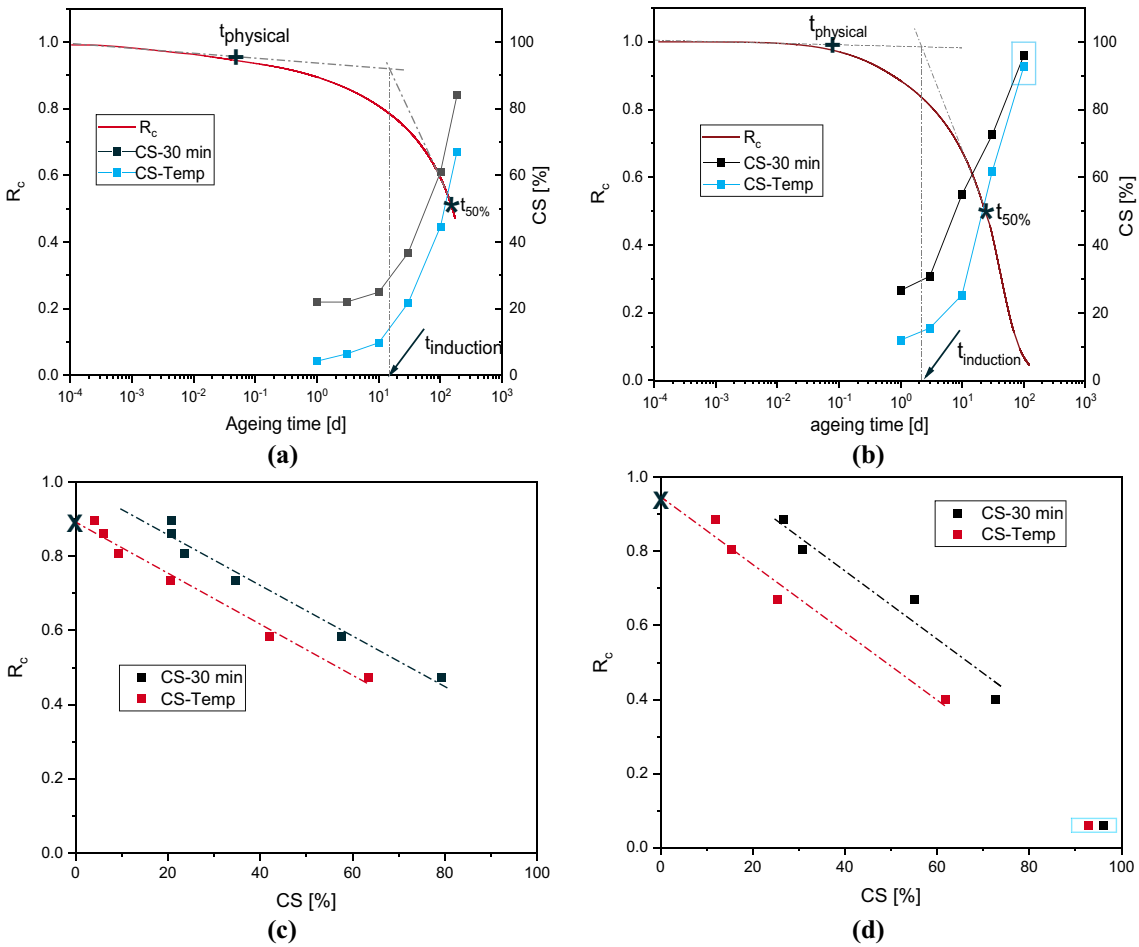

Fig. 5 Normalised compression stress relaxation R_c and compression set CS measurements after 30 min and after tempering. **a** for EPDM aged at 125 ° C and **b** for EPDM aged at 150 ° C. Contribution of physical relaxation to ageing **c** for EPDM aged at 125 ° C and **d** for EPDM aged at 150 ° C Data in the blue square are slightly affected by DLO and therefore excluded from the analysis

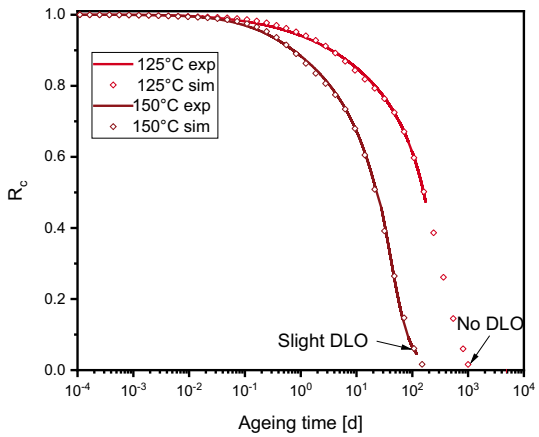

Fig. 6 Experimental and numerical normalised compression stress relaxation results

determined parameters are based on DLO free measurements, the delivered results are also DLO free. From Fig. 3 no DLO effects are detected for samples aged at 909 d and slight DLO effects are noticed after 1093 d. At the ageing interval between 909 and 1093 d where probably DLO effects occur, the Rc values according to our simulation are between 0.03 and 0.004, respectively. So that at 125 ° C ageing temperature, the EPDM ages homogeneously during the SR experiment since the relaxation is almost completed. On the other hand, samples aged at 150 ° C present slight DLO effects after 101 d as shown in Fig. 3. However, as the measured value is very close to the DLO-free simulation, one can suppose that the slight detected DLO effects at 101 d do not significantly affect the measured SR. However, for lower ageing temperatures much longer relaxation times (t_{physical}, $t_{\text{initiation}}$, $t_{\text{induction}}$ and $t_{50\%}$) are to be expected. Taking the example of EPDM aged at 75 ° C, even after 168 d of ageing, the experimental results showed an Rc = 0.88 [26] which is almost within the physical relaxation regime. Similarly, the CS after tempering [21] at this ageing stage was quite low with about 6%. When elastomer components are operated at moderate temperature ranges, physical relaxation should not be neglected. Even at high temperature where chemical processes are dominant, physical processes still contribute to over 10% force drop. With the separation of physical and chemical processes, more reliable lifetime predictions, especially for lower ageing temperatures where samples show slower degradation, can be performed [26] as these predictions are principally governed by the chemical processes.

5 Conclusion

An experimental method to separate physical and chemical relaxation was developed and applied in the present study through the analysis of stress relaxation (SR) and compression set (CS) measurements. An identification strategy for the material parameters based on the relationship between SR and equilibrium CS was proposed. Physical and chemical relaxations were modelled with the Prony series and two decay functions, respectively. This modelling is only valid for homogeneously aged samples which was controlled by the IRHD analysis at different ageing times. However, an extension of the model to take into account DLO effects too is under progress which is applied to another material which degrades faster and experiences DLO effects already during the performed SR measurements (at about $t_{50\%}$).

Acknowledgements Parts of this research were funded by The German Federal Ministry of Economic Affairs and Energy (BMWi, Project No. 1501509) on the basis of a decision by the German Bundestag.

Funding Open Access funding enabled and organized by Projekt DEAL.

Availability of data and materials Not applicable.

Code availability Not applicable.

Declarations

Conflict of interest Not applicable.

References

1. Pervez, T., Al-Jahwari, F.S.: Mechanical properties, sealability, and recyclability of elastomeric materials in petroleum industry. In: Hashmi, S., Choudhury, I.A. (eds.) Encyclopedia of Renewable and Sustainable Materials, pp. 131–147. Elsevier, Oxford (2020). https://doi.org/10.1016/B978-0-12-803581-8.11291-3
2. Balasooriya, W., Clute, C., Schrittesser, B., Pinter, G.: A review on applicability, limitations, and improvements of polymeric materials in high-pressure hydrogen gas atmospheres. Polym. Rev. (2021). https://doi.org/10.1080/15583724.2021.1897997
3. Wolff, D., Völzke, H., Bevilacqua, A., Alejano, C., Conde, J.M., Einziger, R.E., Fukuda, S.I., González Espartero, A., Gouzy-Portaix, S., Haddad Andalaf, R.E., Hambley, D., Issard, H., Kessler, J., Kurpaska, L., Legat, A., Qureshi, A.H., Ruiz, J., Shirai, K., Šmaižys, A., Verrastro, C.A.: Demonstrating performance of spent fuel and related storage system

components during very long term storage - Final report of a coordinated research project. In: González Espartero, A. (eds.) IAEA TecDoc Series. 2019, IAEA Publishing Section: Vienna, Austria, pp. 1–198. https://www.iaea.org/publications/13553/demonstrating-performance-of-spent-fuel-and-related-storage-system-components-during-very-long-term-storage
4. Ehrenstein, G.W., Pongratz, S.: Beständigkeit von Kunststoffen. Carl Hanser, München (2007)
5. Tobolsky, A.V., Frick, N.H., Norling, P.M., Yu, H.: On mechanism of autoxidation of three vinyl polymers-polypropylene, ethylene-propylene rubber and poly(ethyl acrylate). J. Am. Chem. Soc. **86**(19), 3925–3930 (1964). https://doi.org/10.1021/ja01073a004
6. Landi, V.R., Easterbrook, E.K.: Scission and crosslinking during oxidation of peroxide cured EPDM. Polym. Eng. Sci. **18**(15), 1135–1143 (1978). https://doi.org/10.1002/pen.760181503
7. Kömmling, A., Jaunich, M., Wolff, D.: Revealing effects of chain scission during ageing of EPDM rubber using relaxation and recovery experiment. Polym. Test. **56**, 261–268 (2016). https://doi.org/10.1016/j.polymertesting.2016.10.026
8. Tobolsky, A.V., Prettyman, I.B., Dillon, J.H.: Stress relaxation of natural and synthetic rubber stocks. J. Appl. Phys. **15**(4), 380–395 (1944). https://doi.org/10.1063/1.1707442
9. Andrews, R.D., Tobolsky, A.V., Hanson, E.E.: The theory of permanent set at elevated temperatures in natural and synthetic rubber vulcanizates. J. Appl. Phys. **17**(5), 352–361 (1946). https://doi.org/10.1063/1.1707724
10. Johlitz, M., Diercks, N., Lion, A.: Thermo-oxidative ageing of elastomers: a modelling approach based on a finite strain theory. Int. J. Plast. **63**, 138–151 (2014). https://doi.org/10.1016/j.ijplas.2014.01.012
11. Musil, B., Johlitz, M., Lion, A.: On the ageing behaviour of NBR: chemomechanical experiments, modelling and simulation of tension set. Continuum Mech. Thermodyn. (2018). https://doi.org/10.1007/s00161-018-0728-5
12. Mohammadi, H., Morovati, V., Poshtan, E., Dargazany, R.: Understanding decay functions and their contribution in modeling of thermal-induced aging of cross-linked polymers. Polym. Degrad. Stabil. **175**, 109108 (2020). https://doi.org/10.1016/j.polymdegradstab.2020.109108
13. Shaw, J.A., Jones, A.S., Wineman, A.S.: Chemorheological response of elastomers at elevated temperatures: experiments and simulations. J. Mech. Phys. Solids **53**(12), 2758–2793 (2005). https://doi.org/10.1016/j.jmps.2005.07.004
14. Kömmling, A., Jaunich, M., Wolff, D.: Effects of heterogeneous aging in compressed HNBR and EPDM O-ring seals. Polym. Degrad. Stabil. **126**, 39–46 (2016). https://doi.org/10.1016/j.polymdegradstab.2016.01.012
15. Curro, J.G., Salazar, E.A.: Physical and chemical stress relaxation of elastomers. J. Appl. Polym. Sci. **19**(9), 2571–2581 (1975). https://doi.org/10.1002/app.1975.070190919
16. Salazar, E.A., Curro, J.G., Gillen, K.T.: Physical and chemical stress relaxation of a fluoroelastomer. J. Appl. Polym. Sci. **21**(6), 1597–1605 (1977). https://doi.org/10.1002/app.1977.070210615
17. Ito, M.: On the separation of physical and chemical component of stress relaxation. Polymer **23**(10), 1515–1518 (1982). https://doi.org/10.1016/0032-3861(82)90254-3
18. Gillen, K.T., Bernstein, R., Wilson, M.H.: Predicting and confirming the lifetime of o-rings. Polym. Degrad. Stabil. **87**(2), 257–270 (2005). https://doi.org/10.1016/j.polymdegradstab.2004.07.019
19. Wineman, A.: Some comments on the mechanical response of elastomers undergoing scission and healing at elevated temperatures. Math. Mech. Solids **10**(6), 673–689 (2005). https://doi.org/10.1177/1081286505036436
20. Brown, R.P., Forrest, M.J., Soulagnet, G.: Long-term and accelerated ageing tests on rubbers. Rapra Technology Limited, Shrewsbury (2000). http://hdl.handle.net/10068/646890
21. Kömmling, A., Jaunich, M., Goral, M., Wolff, D.: Insights for lifetime predictions of O-ring seals from five-year long-term aging tests. Polym. Degrad. Stabil. **179**, 109278 (2020). https://doi.org/10.1016/j.polymdegradstab.2020.109278
22. Zaghdoudi, M., Kömmling, A., Jaunich, M., Wolff, D.: Scission, cross-linking, and physical relaxation during thermal degradation of elastomers. Polymers **11**(8), 1280 (2019). https://doi.org/10.3390/polym11081280
23. Johlitz, M., Retka, J., Lion, A.: Chemical ageing of elastomers: experiments and modelling. In: ECCMR- Constitutive Models for Rubber, Dublin (2012)
24. Vohlídal, J.: Polymer degradation: a short review. Chem. Teach. Int. **3**(2), 213–220 (2021). https://doi.org/10.1515/cti-2020-0015
25. Bernstein, R., Gillen, K.T.: Predicting the lifetime of fluorosilicone o-rings. Polym. Degrad. Stabil. **94**(12), 2107–2113 (2009). https://doi.org/10.1016/j.polymdegradstab.2009.10.005
26. Zaghdoudi, M., Kömmling, A., Jaunich, M., Wolff, D.: Erroneous or Arrhenius: a degradation rate-based model for EPDM during homogeneous ageing. Polymers **12**(9), 2152 (2020). https://doi.org/10.3390/polym12092152